Chapter 1

New perspectives on intermediate phases

P. Boolchand[a], Ping Chen[a], Deassy I. Novita[a], B.Goodman[b]

[a]*Department of Electrical and Computer Engineering, University of Cincinnati, Cincinnati, OH 45221-0030, USA*
[b]*Department of Physics, University of Cincinnati, Cincinnati, OH 45221-0011, USA*

Disordered networks of covalent, ionic and H-bonded solids acquire unusual functionalities in *intermediate phases* (IPs), which form in a narrow but well defined range of connectivity. Their chemical bonds apparently self-organize, i.e., globally adapt through reconnecting so as to expel stress and lower their free energy. IPs are now classified as marginally rigid structures and usually are made up of more than one isostatic local molecular units. We have recently come to appreciate that they possess liquid-like entropies, i.e., undergo a minimal change in configurational entropy upon structural arrest from the liquid state. These features of IP glasses are thought to be responsible for their non-aging behavior and optimal glass forming tendency.

1.Historical

A significant step forward to understanding glasses at a basic level emerged in the early 1980s, when J.C.Phillips [1] and M.F.Thorpe [2] predicted that a *flexible* network upon progressive cross-linking will become *rigid* at a magic connectivity, $\boldsymbol{r} = 2.40$. In covalent networks atoms usually bond in conformity with the 8-N rule, and the mean coordination number $\boldsymbol{r}$ can be estimated,

$$\boldsymbol{r} = \left(\sum_i n_i r_i\right) \Big/ \left(\sum_i n_i\right) \qquad (1)$$

Series: Optoelectronic Materials and Devices, ISSN 1584-5508
Volume 6, 2009, Rigidity and Boolchand intermediate phases in nanomaterials, ISBN 13/978-973-88109-4-5

Here n_i and r_i designate the concentration and coordination number of i^{th} atom, as forming part of a network. For networks that are fully polymerized, i.e., there are no demixing effects, $\boldsymbol{r}$ serves as a faithful measure of network connectivity. The prediction is based on the simple and elegant idea that in covalent networks bond-stretching and bond-bending forces act as mechanical constraints. Ideas on constraints in mechanics go back to the work of J.L. Lagrange [3] in 1788. And when the count of these constraints per atom equals 3, networks become elastically rigid as $\boldsymbol{r}$ increases to 2.40. J.C. Maxwell [4] had used such counting algorithms to determine stability of mechanical structures such as trusses and bridges in 1864. Numerical simulations [5] on *random* networks based on depleted amorphous Si as models of glasses have provided support for these ideas. Early experimental evidence for onset of rigidity in chalcogenide glasses came from measurements of Lamb-Mossbauer factors [6-8]. Binary Ge_xSe_{1-x} glasses are particularly attractive systems for these studies because one can reproducibly change connectivity $\boldsymbol{r}$ over a wide range, $2 < \boldsymbol{r} < 2.67$ by tuning the stoichiometry 'x' of glasses. Measurements of ^{119}Sn Lamb-Mossbauer factors revealed [6] atomic mean-square displacements to be large in flexible networks (such as Se glass; x = 0), these displacements to steadily decrease as networks are cross-linked, and to saturate once x exceeded 20%, corresponding to $\boldsymbol{r} = 2.40$, the rigidity transition. In subsequent years more stringent experimental tests were undertaken, and it emerged, starting in 1997, that there was not one (elastic phase transition) but in fact <u>two</u> [9, 10] elastic phase transitions. Raman scattering experiments complemented by calorimetric ones on binary Si-Se [9, 11] and Ge-Se [10] revealed that structure of these network glasses over a range of connectivity near $\boldsymbol{r} \sim 2.40$ evolves in a far richer fashion [12] than merely random.

These findings, supported by numerical simulations [13] on self-organized networks have suggested that with increasing connectivity, ($\boldsymbol{r}$), the first transition is the *rigidity* transition ($\boldsymbol{r_1}$), while the second one is the *stress* transition ($\boldsymbol{r_2}$). Thus, as a Se chain network is steadily cross-linked by alloying Si or Ge, rigid regions of the network begin to percolate as $\boldsymbol{r}$ increases to $\boldsymbol{r_1}$ (= 2.40). And with a further increase of connectivity $\boldsymbol{r}$ (> $\boldsymbol{r_1}$), networks are able to collectively reconnect and expel stress nucleating redundant bonds [14] to lower their Gibbs free energy. A point is then reached at $\boldsymbol{r} = \boldsymbol{r_2}$ (= 2.52), when redundant bonds can *no longer* be excluded by reconnecting networks; stress then permeates and a first order transition is manifested as $\boldsymbol{r}$ exceeds $\boldsymbol{r}_2$. The phase formed between the onset of rigidity and that of stress, henceforth denoted as the intermediate phase (IP) is rather unusual; it is found to be rigid but stress free. The stress-free character of the IP in binary Ge-Se glasses has now been independently demonstrated in pressure Raman experiments [15]. IP glasses possess the feature that their chemical bonds can globally reconnect to form stress-free networks, a *new functionality* that is identified with *self-organization* [16]. The physical

behavior of Intermediate Phase (IP) [9, 12, 17-21] glasses as being distinct from *flexible phase* glasses formed at $r < r_1$, and *stressed-rigid phase* glasses formed at $r > r_2$ emerged in calorimetric, photostructural, electrical and Raman optical elastic measurements, and we will review these in the present work. Numerical simulations on 2D triangular networks[14] 22, 23] , and also on 3D networks based on depleted amorphous Si [13] have shown the existence of such a phase in these idealized systems. These results have also stimulated interest in the more formidable task of modeling chalcogenide glasses using numerical simulations. Investigations of the nature of the IP in real glasses are an exponentially complex problem, but also a rewarding one. It may provide insights into how networks *adapt* to expel stress, a functionality that will have an impact much beyond glass science.

IPs display a number of remarkable properties, the more notable being their stress-free character resulting in little or no aging [18, 20], in contrast to glass compositions outside IPs that are found to age. The metastability and dynamic reversibility of IPs was not predicted, but it is of great importance in not only practical applications [22] but also in challenging our ideas about the glass transition [22, 23].

One cannot help but remark that developments in the field of glass science over the past decade have led to complete re-thinking of structure of network glasses since the early work of Zachariasen [24]. In his celebrated paper, Zachariasen described the structure of stoichiometric oxides such as SiO_2 and B_2O_3 to be examples of continuous random networks. While such a description may well be appropriate for select stoichiometric oxides, for many modified oxides and covalent glass systems, experiments have now shown these glass systems to be neither *chemically ordered*, nor fully *connected* and, within a range of connectivity, their structures to evolve not even in a *random* fashion.

It is timely, indeed, that Professor M. Popescu and Professor M. Micoulaut have organized the current volume that explores facets of this new phase of disordered condensed matter. Applications of amorphous or glassy solids would benefit from the quasi-equilibrium nature of structures formed in IPs. The interaction of pair-producing radiation with glass compositions in the IP also appears to be quite special, and it may well be a consequence of the stress-free nature of structures formed in IPs.

2. What is new on Intermediate Phases?

We comment on the broader implications of IPs in section 6. Here we focus on some new findings on IPs in glass science**.**

2.1 Experiments

In the past three years several new developments in the field have taken place both in theory and experiment. On the experimental side some of these developments are as follows. **(i)** IPs were first reported in group IV (Ge,Si) and group V (As, P) selenides. These have now been observed in some group V sulfides, and the results are quite unexpected; IPs in these sulfides are shifted to lower ***r*** in relation to those in corresponding selenides. In the IP of the sulfides, S_8 rings and $(As \text{ or } P)_4S_4$ or $(As \text{ or } P)_4S_3$ molecules are nearly absent, S_n chain bearing backbones do not always form fully polymerized networks, and some S_n chain fragments decouple from the backbone. These demixing effects appear to be partial in the As-S binary system, but almost complete in the P-S binary. The composition of the IP centroids is determined by connectivity of their backbones. **(ii)** In sharp contrast, ternary selenides and sulfides containing equal proportions of group V and group IV elements display very similar IPs. The S_n chain demixing effect alluded to above does not seem to occur in these ternary systems. The group IV cation apparently stitches back the demixed S_n chains to promote polymerization of the sulfides like the selenides. **(iii)** Amorphous thin-films of the chalcogenide also show IP features. Recent work [25] has shown a close connection between the IP of the Ge_xSe_{1-x} binary and giant photocontraction effects in obliquely deposited amorphous thin-films. **(iv)** IPs have now been observed in mixed covalent-ionic systems such as the modified oxides (alkali silicates and alkali germanates) and the fast-ion conducting glasses ($AgI\text{-}AgPO_3$). This adds an electrical feature to the now familiar thermal and optical signatures of IP networks.

These new developments suggest that classification of glasses based on their elastic response in terms of the three regimes, flexible, intermediate and stressed-rigid is not confined to covalent networks but may well be a *generic* feature of the disordered state of matter.

2.2 Theory

Theoretical contributions addressing different aspects of the IP appear in several chapters of this book including chapters 2 and 4 through 10. What is special about them topologically as network structures? How to understand their mechanical rigidity and vibrational properties, etc? The remainder of this section introduces a possibly essential new ingredient which should be incorporated into theoretical analysis.

The idea is that m-DSC, which has been so powerful as a probe of the IP, measures essentially the *configurational entropy change* during the glass-melt transition at T_g or, specifically, it is given directly by the non-reversing enthalpy at T_g. The notion of configurational entropy (S_c) for a glass or liquid has intuitive appeal and has been around for a while. It is often used in connection with the landscape picture, namely, the fictive plot

in configuration space of the potential energy V{q}, where {q} is the collective coordinate set. Thus, for estimating the rate of collective rearrangements, the number $\Omega(\varepsilon)$ of metastable minima at the energy ε is needed; and $S_c = k_B \ln \Omega(\varepsilon)$. The kinetic thermal energy is assumed to reside along with vibrational potential energy in approximately (anharmonic) oscillatory motion within the metastable potential wells, and also in the velocities at the Eyring-type transition states involved in rearrangement processes between wells. The oft quoted Adams-Gibbs [26] relaxation time formula invokes configuration entropy, namely,

$$\tau^{-1} = A \exp(-B/TS_c) \tag{2}$$

where S_c is configuration energy per mole. (A comment in passing: There is an apparent ambiguity in connection with this formula in that the coefficient B contains a configuration term also. The transition state kinetic energy appears in the coefficient A). Separating the system entropy into kinetic and configuration parts is of *conceptual* use as shown in Eq. (2). As stated above, it is also of particular empirical relevance here in connection with m-DSC experiments. In an m-DSC experiment of the glass melting transition, the applied temperature increase has a linear ramp and an oscillatory part, namely,

$$T(t) = T_o + at + b\sin\omega t \tag{3}$$

(See section 3 for more particulars). It is unlikely that a clean separation can be made of the changes around T_g, the glass transition temperature into vibrational thermal changes and a structural rearrangement part. But, nevertheless, it is a valuable perspective [27] and gives us a useful way to interpret m-DSC data. For one thing, thermal kinetic energy resides mostly in anharmonic vibrational motion (along with vibrational potential energy). The kinetic energy associated with transition states during rearrangements, activated or otherwise, is probably much smaller. Some insight into the complexity of these changes may be gleaned from recent computer studies of a model binary 2D liquid of interacting discs near the freezing temperature - which seems to show both a separation of and, at the same time, a subtle interplay of vibrational motion and irreversible rearrangements where a significant number of molecules is involved [28]. In particular, low frequency multi-unit modes seem to persist through the irreversible local rearrangements. This suggests our 'ansatz' below, namely, that the changes of modal kinetics with temperature is relatively reversible even in the presence of irreversible local re-arrangements.

Under a small temperature change δT the heat uptake δH should then divide into reversible (recoverable) and irreversible parts, which we

write as,

$$\delta H = h_r \delta T + \not\delta_{nr} H \tag{4}$$

The quasi-differential symbol $\not\delta_{nr}$ is similar to the notation used for the thermodynamic relation for a small addition of heat

$$\not\delta q = du + dw \tag{5}$$

which designates that there is no heat function of state q(T) and that reversible cycle will not restore q; but rather it is the entropy S(T) which is restored.We do not have a mathematical formulation for $\not\delta_{nr} H$ but its connection to the irreversibility of temperature-induced structural changes suggests that, in a sinusoidal T-cycle of small amplitude, $\not\delta_{nr} H$ is highly hysteretic and will cycle with an amplitude quite a bit less than $h_r \delta T$. Then we can identify h_r with a reversible specific heat $C_p(T)$ at that momentary temperature in the glass transition. In m-DSC, where the programmed temperature is given by equation (3), C_p can be determined from the corresponding sinusoidal amplitude of modulated heat flow [29]. The integrated heat input, averaged over the temperature cycles, is then

$$\Delta H(T) = \int_{T_0}^{T} C_p(T) dT + \int \not\delta_{nr} h = \Delta H_r + \Delta H_{nr} \tag{6}$$

The entropy change from T_o to T is

$$\Delta S(T) = \int_{T_0}^{T} \frac{\delta H}{T} = \int_{T_0}^{T} \frac{C_p(T)}{T} dT + \int \frac{\not\delta_{nr} H}{T} \tag{7}$$

where, again, from the interpretation earlier of $\not\delta_{nr} H$ as measuring the heat going into irreversible structural changes, we write

$$\Delta S = \Delta S_k + \Delta S_c \tag{8}$$

where ΔS_k denotes change in vibrational entropy and ΔS_c denotes change in configurational entropy encompassing T_g. In the landscape picture, since higher metastable minima will be important at higher temperatures both S_c and S_k depend on temperature.

Thus, almost fortuitously, m-DSC yields an experimental number for the computationally elusive S_c and leads to a remarkable entropic characterization of the IP. The change in S_c from the solid glass to liquid melt is

$$S_{c\,liq} - S_{c\,gl} = \int_{T_{gl}}^{T_{liq}} \frac{\not\delta_{nr} H}{T} \tag{9}$$

And since the change $T_{liq} - T_{gl}$ through the glass transition is small (40K) compared with T_g (~ 300K -1000K), we can write

$$\Delta S_c = S_{c\,liq} - S_{c\,gl} \cong \frac{\int \not{\delta}_{nr} H}{T_g} = \frac{\Delta H_{nr}}{T_g} \qquad (10)$$

This is the central result.

Outside the IP the change ΔS_c across T_g is of the same order as liquid entropy. This reflects the considerably reduced configurational freedom on freezing. But in the IP the very small non-reversing heat flow tells us that the glass and liquid have almost the same configurational freedom. So the IP is a high entropy phase! We illustrate the idea schematically in Fig. 1, which shows changes in configurational entropy near T_g for the three types of elastic phases encountered in studies on network glasses. This seems to confound the generally held impression to the contrary. The theoretical challenge is to calculate ΔS_c in the IP and also

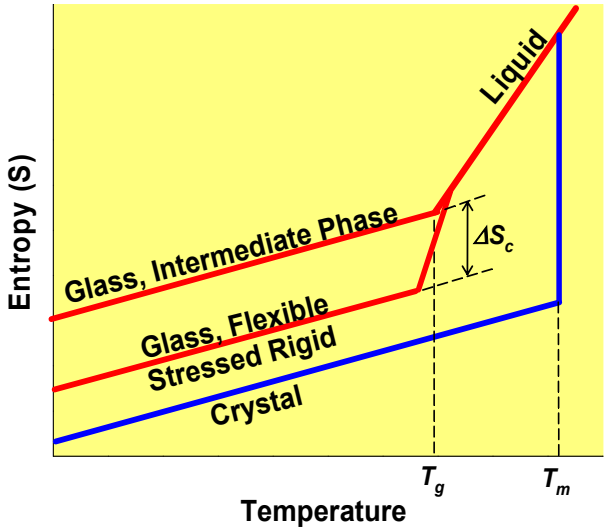

Fig. 1. Normal liquids crystallize at T_m, while glass forming liquids can be supercooled to undergo structural arrest at a lower temperature-T_g. Intermediate Phase glasses possess higher entropy than those of flexible or Stressed Rigid glasses. Adapted from [30].

to understand why it is so much smaller than its value in compositions outside the IP - which correspond to the fragile liquid compositions .

We can only speculate at this stage that a key feature behind the

high entropy is its homogeneous constraint distribution. Each molecular unit is isostatic ($< n_c > = 3$). Then, on the size scale of a unit, there is a homogeneous distribution of *exactly* 3 Lagrangian constraints per atom *with no fluctuation.* This homogeneity is broken in the stressed-rigid phase by the presence of redundant bonds. Support for this idea lies in the finite compositional width of IPs shown in Fig. 6. which is due to the simultaneous presence in the phase of more than one isostatic chemical unit. Refer, for example, to the corner- and edge- sharing units in binary Ge-Se glasses and the pyramidal- and quasi-tetrahedral-units in binary As-S glasses (see Fig. 11). The homogeneity of isostaticity apparently facilitates rearrangement in structures of these units near T_g in the glass - like in the melt; while redundant bonds inhibit structural rearrangement. In this connection we note that the pressure *threshold* seen only outside the IP in the pressure-induced shifts of the Raman mode frequency of corner sharing tetrahedra [15] in Ge-Se glasses has been attributed tentatively to an inhomogeneous network structure containing mixed both isostatic and overconstrained subnetworks in contact; and another relevant observation is the microscopic inhomogeneity evident outside the IP in birefringence of modified oxide glasses, [31] which is absent within the IP. It will be of interest to study how the liquid-like entropy in the IP changes at temperatures well below T_g. For example, if S_c continues to be relatively high compared to the non-IP compositions, it will reinforce the challenge of the singular nature of the IP glass phase.

How does the view above T_g correlate with the view below T_g? Fairly complete results on the activation energy of viscosity at T_g, ΔE_a, in the As_xSe_{1-x} binary [32] and the $Ge_xAs_xSe_{1-2x}$ ternary are now available. In Fig. 2 the dimensionless liquid 'fragility', which is $m = \Delta E_a/k_BT_g$, is compared with the variation of the non-reversing enthalpy at T_g, $\Delta H_{nr}(x)$, from mDSC experiments (open circles). It is clear that the window in $\Delta H_{nr}(x)$ *coincides* with the strong-liquid regime in the fragility. Thus, in covalent systems, IP glasses upon heating give rise to *strong* liquids, while glass compositions outside the IP range give rise to *fragile* liquids; so the stress-free nature of glasses in the IP apparently extends in some way to liquid dynamics. This correspondence is added to the challenge of understanding structural entropy. When *strong* liquids are cooled to T_g, dynamical structural correlations must grow in length scale as ideal glasses possessing marginally rigid stress-free networks form in the IP. Now, there are different theoretical descriptions of glass formation from the melt, such as the mode-coupling view [33, 34] of solidification as a continuous slowing down of correlations of increasing range. Since these theories do not anticipate the long-range entropy state of the IP, they must be considered as too generic to explain *real* glasses.

3. Experimental probes of intermediate phases

Intermediate phases (IPs) have been observed in experiments on glasses and amorphous thin-films. Some of these, experiments include calorimetric, light scattering and ion-conduction. The calorimetric measurements can be applied to any glass system, in general and these have

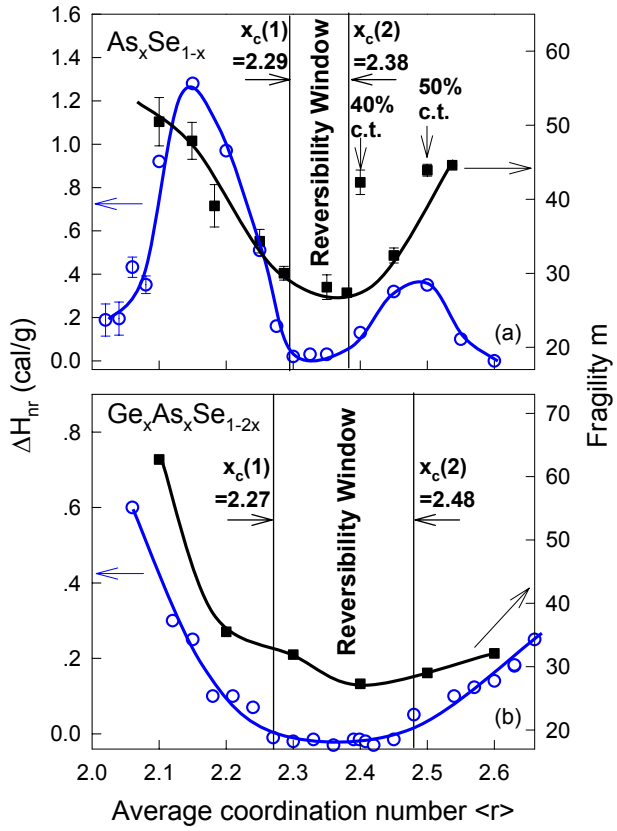

Fig. 2. Variations in liquid fragilities (m(x)) and non-reversing enthalpy at T_g, $\Delta H_{nr}(x)$as a function of glass compositions for (top) binary As_xSe_{1-x} glasses and (bottom) ternary $As_xGe_xSe_{1-2x}$ glasses taken from ref [16, 35].Noteworthy is that the window in $\Delta H_{nr}(x)$ coincides with the window in liquid fragilities, m(x).

yielded rather provocative results that not only have a bearing on IPs but also on understanding the elusive nature of glass transition [36].

3.1 Modulated differential scanning calorimetry

Glass transition temperatures (T_gs) have routinely been measured using differential scanning calorimetry (DSC) over the past 40 years. One usually observes an endothermic step with an overshoot, as the heat uptake of a glass sample is registered when it is heated at a given scan rate of typically 10°C/min. One localizes the glass transition temperature, T_g , by inflection point or mid-point of the step [37]. In practice there are difficulties. First, the nature of the overshoot that accompanies the step is not always certain how to analyze. Second, the kinetic nature of T_g leads, in general, to a shift of T_g to higher temperatures as scan rates are increased. At low scan rates (< 5°C/min), kinetic shifts become small but signal to noise ratio also decreases, since signal strength depends on scan rates (dT/dt) linearly. Modulated-DSC, a more sensitive variant [29, 38], was introduced in the mid 1990s and its use has permitted overcoming many of these limitations [29, 38]. In this approach, one programs a sinusoidal temperature modulation over the linear temperature ramp, and deconvolutes the total endothermic heat flow into two components; one that tracks the modulations, called "reversing heat flow: dH_r/dt", and a second signal obtained by subtracting the total heat flow from the reversing heat flow, called "non-reversing heat flow: dH_{nr}/dt". (In conformance with common convention the / denoting quasi-differentials is omitted.) Thus, the total heat flow in a glass sample can be written as,

$$dH_t/dt = dH_r/dt \; (= C_p dT/dt) + dH_{nr}/dt \qquad (11)$$

Since mDSC is an AC method, the full power of phase sensitive lock in detection is used to extract small signals at low scan rates. One obtains scan rate independent T_gs. Accurate measurements of T_gs serve as useful check of sample heterogeneity [39], and the variation of T_g with chemical composition yields profound insights in glass structure (see below). More importantly, the endothermic overshoot experiments reveal, forms part of a Gaussian-like peak that belongs to the non-reversing heat flow. The reversing heat flow signal appears as a rounded step-like jump, and one fixes T_g by its inflection point [22]. The separation of the reversing from the non-reversing heat flow is fundamentally an important development in glass science; the reversing heat flow relates to ergodic events and thermodynamics (including measurements of C_p in the glassy or liquid state), while the non-reversing heat flow relates to non-ergodic events such as configurational changes accompanying structural arrest near T_g. M-DSC can also be used in the frequency domain, and such experiments have shown [40] that these results are a low frequency extrapolation of traditional AC calorimetry [41, 42].

3.1.1.Three types of glass transitions

Experiments on a wide variety of covalent glasses (more than 100 samples) have shown that there are, in general, three types of glass transitions. The *first* type is usually observed in flexible glasses such as Se-rich binary and ternary alloys, and it is characterized by a non-reversing heat flow that is Gaussian-like, symmetric, narrow (typically 20°C wide), with the integrated area under the Gaussian profile (ΔH_{nr}) slowly increasing as a function of waiting time for samples held at $T < T_g$, i.e., the non-reversing enthalpy term slowly ages. The *second* type of glass transition is found in glasses that are rigid but unstressed, and it consists of a ΔH_{nr} term that is not only minuscule but also does not age much. The second type of glass transition leads to T_gs that are largely thermally reversing or non-hysteretic in character, a feature characteristic of IPs (see below). Finally, the *third* type of glass transition is encountered in stressed-rigid glasses, and it usually displays a dH_{nr}/dt profile that is broad (typically 40°C wide), asymmetric with a high temperature tail, with the underlying enthalpy (ΔH_{nr}) increasing with waiting time, i.e., the term ages. In summary, it is now possible to identify the nature of the elastic phase of a glass sample, i.e., either flexible, or intermediate or stressed-rigid, from a measurement of glass transition endotherm in an m-DSC experiment [22, 43].

3.1.2 Compositional trends in T_g and glass structure.

Changes in T_g resulting due to those upon chemical alloying a base glass B, with an additive A, such as a binary A_xB_{1-x} system, have been examined by several groups [44-47]. These effects are much larger than changes in T_g brought about by changing quench rates. We provide two examples, one of an oxide and the other of a chalcogenide glass. Addition of 4 mole % of Na_2O to SiO_2 base glass leads to a rather spectacular drop of T_g from about 1200°C to 850°C. In binary Ge_xSe_{1-x} glasses, as x increases to 10%, T_gs increase from 40°C to 120°C. Several workers have attempted to build structural models to understand these variations. One particular approach, Stochastic Agglomeration Theory [47], has attracted particular attention because it can predict slopes of changes in T_g with glass composition. For the two examples given above, the *parameter free* slopes predicted by SAT agree with experiments rather well. These data reveal that variations in T_g with glass composition are determined by those in network connectivity, thus underscoring the importance of glass structure evolution.

In Fig. 3, we reproduce the compositional variation of $T_g(x)$ and the non-reversing enthalpy at T_g in binary Ge-Se glasses [48]. The increase of T_g with x reflects the increased crosslinking of Se_n chains by the 4-fold Ge additive. But as x increases to near 33.33%, T_g displays a global maximum near the chemical threshold. The nature of the threshold has been widely

debated [49]. One view is that it constitutes evidence of nanoscale phase separation, i.e., Ge-Ge bonds formed at x > 33.33% demix from the backbone to form part of second Ge-rich nanophase.

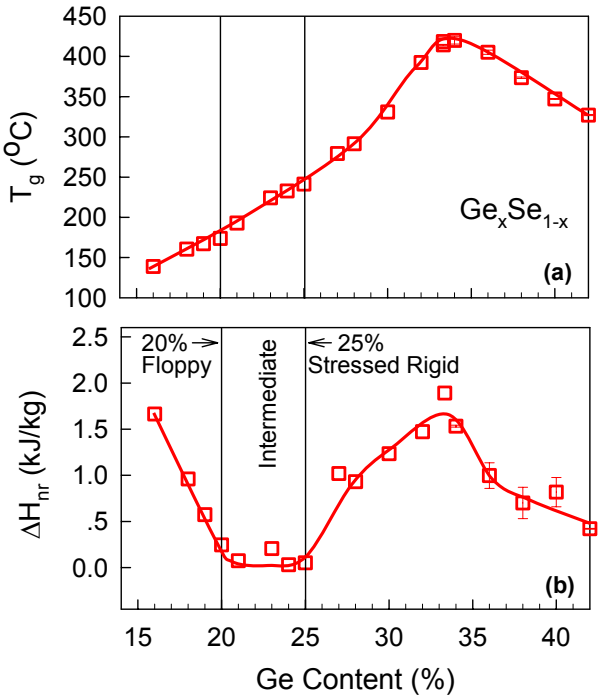

Fig. 3. Variations in (a) glass transition temperature, $T_g(x)$ and (b) non-reversing enthalpy, $\Delta Hnr(x)$ in binary Ge_xSe_{1-x} glasses taken from the work of Ping Chen [48]. Similar results were obtained by F. Wang et al. [15].

The structural feature leads to a loss of network connectivity, which is reflected in T_g decreasing with x. Detailed spectroscopic and thermal experiments [50] on glasses as a function of composition reveal, the slope dT_g/dx to show a maximum exactly at the composition where Ge-Ge bonds are first manifested in these binary glasses near x = 31%. An alternate view is to identify the threshold in $T_g(x)$ to weaker strength of bonds formed above the threshold (Ge-Ge) compared to the stronger ones (Ge-Se) prevailing below the threshold. If connectivity of networks indeed controls T_g, one must then ask, what role, if any, do chemical bond strengths play [51] to determine T_g of glasses? We address the question next.

3.1.3. Chemical bond strengths and T_g.

There is substantial evidence to suggest that for networks possessing the same connectivity, T_gs scale with chemical bond strengths. Thus, for example, GeS_2 and $GeSe_2$ glasses represent examples of stoichiometric glasses that are largely composed of nearly fully polymerized structures of S or Se bridging Ge(Se or $S_{1/2})_4$, tetrahedral units. In these AB_2 systems, a simple count of mean coordination number gives $\boldsymbol{r}$ = 2.67. The T_g of GeS_2 glass of 508 ^oC (781 K) is 13.3% higher than the T_g of $GeSe_2$ glass of 416 ^oC (689 K). The result can be reconciled with the 13.1% higher chemical bond strength [52] of Ge-S bond (55.52 kcal/mol) over Ge-Se bond (49.08 kcal/mol). In Fig. 4 we compare compositional variation of T_g in ternary $Ge_xP_xS_{1-2x}$ glasses with corresponding selenides. We find that in the 10% < x < 18% range, a chemical bond strength rescaling of T_g occurs; the 13% higher T_g of sulfide glasses correlates well with the 13% stronger chemical bonds of Ge and P with S in relation to corresponding bond strengths of

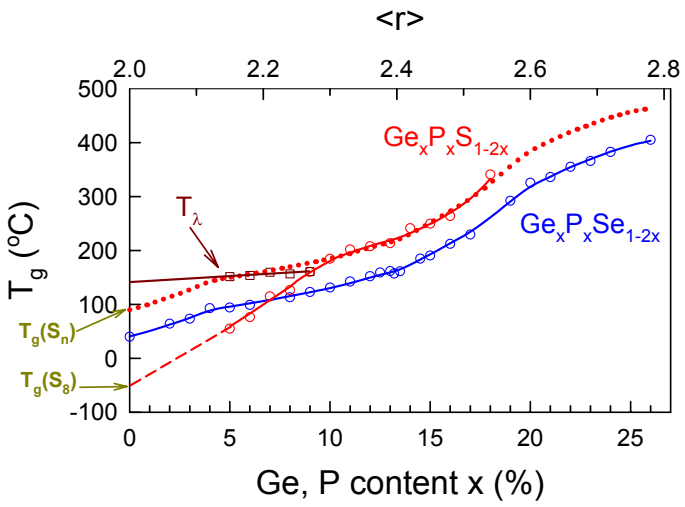

Fig. 4. Compositional variation of T_g (x) in ternary Ge_xP_x(Se or S)$_{1-2x}$ glasses showing a bond strength rescaling in the 10% < x < 18% range where network structure and connectivity reveal ommonality. Figure taken from ref. [53].

these cations with Se. [53, 54] At x < 10%, such rescaling of T_g does not hold Such chemical bond strength rescaling of T_g is also conspicuously absent in comparing the binary As-S glasses with As-Se ones in the range where network because the sulfide glasses demix into S_8 rings leaving a S-deficient backbone. formation occurs, suggesting that underlying connectivity of their backbone structures must be different [53, 54].

3.1.4 Reversibility windows and intermediate phases.

Perhaps the most striking result to emerge from m-DSC experiments bears on the compositional variation of the $\Delta H_{nr}(x)$ term, which display global minima over a range of compositions, as illustrated for example for the case of the Ge_xSe_{1-x} binary system in Fig. 3. In the range of compositions $20\% < x < 25\%$, glass transitions become almost

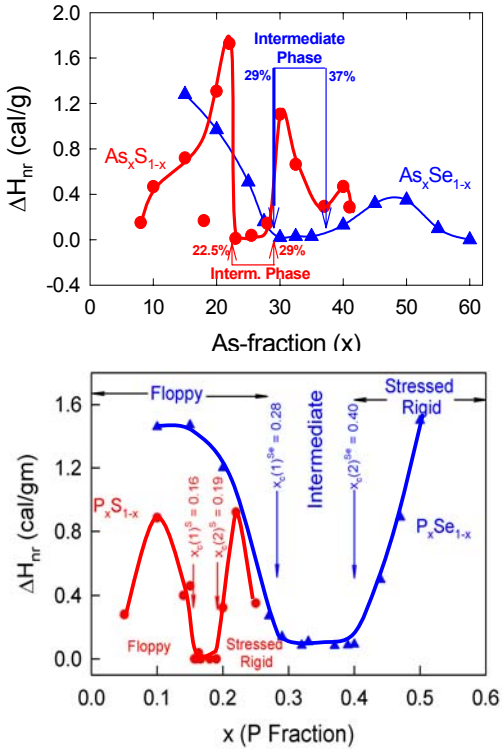

Fig. 5. Variations of the non-reversing enthalpy at Tg in (a) P-S (●) and P-Se (▲) binaries and (b) in As-S (●) and As-Se (▲) binaries revealing the reversibility windows. These data are taken from ref. [53].

completely thermally reversing, and for that reason the composition interval is often referred to as the *reversibility window* (RW). We identify these windows with Intermediate Phases in these chalcogenides. The assignment is corroborated from Raman optical elasticity is corroborated from Raman optical elasticity measurements, and will be described in next section In the Ge_xSe_{1-x} binary, since the coordination numbers of Ge and Se are 4 and 2, one can show $\boldsymbol{r} = 2\ (1 + x)$, and the RW

translates into a network connectivity that spans the range, $2.40 < \boldsymbol{r} < 2.50$. There are two types of Ge centered local structures that are isostatic and thought to contribute to the formation of the stress-free backbone in this binary; corner-sharing $GeSe_4$ tetrahedra corresponding to $\boldsymbol{r} = 2.40$, and edge sharing $GeSe_2$ tetrahedra corresponding to $\boldsymbol{r} = 2.67$. The extension of the RW to a range of $r > 2.40$ is broadly supported by constraint counting algorithms applied to clusters composed of these local structures [55].

In Fig. 5 we show results of RWs in the group V chalcogenides [53]. In these systems, one can show that $\boldsymbol{r} = 2 + x$, when the group V elements is either 3-fold or 4-fold coordinated. A perusal of the data reveals that RWs now extend to a range of $\boldsymbol{r}$ that lies below 2.40. For example, RWs in the two group V-selenides, P_xSe_{1-x} and As_xSe_{1-x}, are found to reside in the $28\% < x < 40\%$ range, i.e., $2.28 < \boldsymbol{r} < 2.40$ range. Here it is remarkable that the RWs coincide for these two selenides, a feature that must reflect an underlying

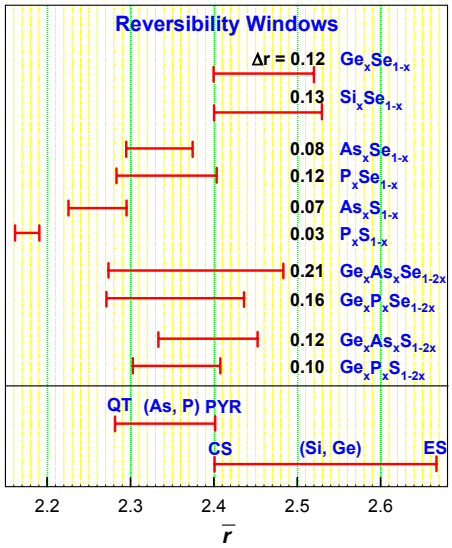

Fig. 6. Reversibility windows in titled glasses shown as a bar chart, with the length of the bar showing the range in connectivity space measured in terms of r, the mean coordination number.

commonality of glass structure. We also note that RWs in corresponding sulfides, i.e., P_xS_{1-x} and As_xS_{1-x} , are shifted to lower x in relation to corresponding Selenides. The shift of the window to lower x is greater for the P- S binary ($16\% < x < 19\%$) than for the As-S binary ($23\% < x < 28\%$). What aspects of structure contribute to the observation? The two relevant isostatic local structures that contribute to RWs in the group V chalcogenides are pyramidally ($Pn(S_{1/2})_3$) and quasi-tetrahedrally ($S{=}Pn(S_{1/2})_3$)

coordinated Pnictide, Pn= As or P centered local structures. These two local structures, possess respectively a chemical stoichiometry of $\boldsymbol{r}$ = 2.40 and 2.28, and for that reason these windows are now shifted to r < 2.40.

We conclude this section with a final comment. The RWs in ternary alloys comprising of both Group IV and group V elements with the chalcogenides have also been measured and these are found to possess rather large widths. For example, the RW in ternary $Ge_xAs_xSe_{1-2x}$ glasses is one of the widest reported to date (figure 6). In this figure, we have included observed RWs in several chalcogenide glasses as a bar chart that encompasses the range of network connectivity or $\boldsymbol{r}$ range spanned. One can see from the data of Figs. 5 and 6 that the RW in the Ge-As-Se ternary is approximately the sum of windows in the As-Se
and Ge-Se binaries. These data are suggestive that widths of RWs are determined by the stoichiometry of specific local structures that contribute to the RWs. The centroid of RWs, on the other hand, appears to be tied to the degree of network polymerization. We discuss the issue in section 5.

3.2 Optical and acoustic probes

Brillouin scattering [56], Raman scattering [57] and IR reflectance [54] have proved to be particularly powerful probes of elastic phase transitions in covalent systems. Brillouin scattering probes solids, in general, on a length scale usually set by the wavelength of acoustic modes. In the case of the present covalent glasses, it is the 30 nm range. For this reason, Brillouin scattering can only serve as a mean field probe of elastic behavior. For that reason one does not expect to observe IPs [58], nevertheless rather remarkable photo-acoustic softening effects are observed when glassy networks become stress-free [56]. Raman and IR reflectance probe glass structure through optical vibrational modes that are more localized and usually display vibrational features that are reasonably narrow and well resolved in many cases. These light scattering probes have proved to particularly useful probes of Ips [19].In the Ge-Se binary for example, three distinct vibrational modes are observed, one near υ_{CS} = 200 cm^{-1} identified with a symmetric stretch of CS tetrahedra, one near υ_{ES} = 217 cm^{-1} identified with a stretch of ES tetrahedra and finally one near υ_{Se} = 250 cm^{-1} identified with stretch of chains of Se_n. Although the frequency of these modes on an absolute scale is set by bond-stretching and bond-bending force constants, small increments in mode frequencies in a network result due to increased cross-linking of the underlying tetrahedral. As networks stiffen upon crosslinking one expects mode frequencies to blue shift in general. By systematically measuring Raman mode frequency of CS modes (υ_{CS}) over a wide range of glass compositions, one can identify three domains of variation. At low x, mode frequencies steadily increases as glasses slowly age. At intermediate x, mode frequencies, υ_{CS} (x), vary almost linearly with x. And finally at high x, υ_{CS} (x) varies as a power-law in x. In figure 7, the

top panel (a) shows a plot of the variation in υ_{CS} (x) for the case of the $Ge_xAs_xSe_{1-2x}$ ternary. Variation of the non-reversing enthalpy at T_g , $\Delta H_{nr}(x)$ in these glasses are plotted in the bottom panel (b). A striking feature of the data of Fig. 7 is the close connection between thermal and optical measurements, both of which reveal three domains of variations in x. These experiments supported by numerical simulations [13] have shown that the first threshold at $x_1 = 9\%$ or $r_1 = 2.27$ and the second threshold $x_2 = 16\%$ or $r_2 = 2.48$ represent respectively the "rigidity" and "stress" elastic phase

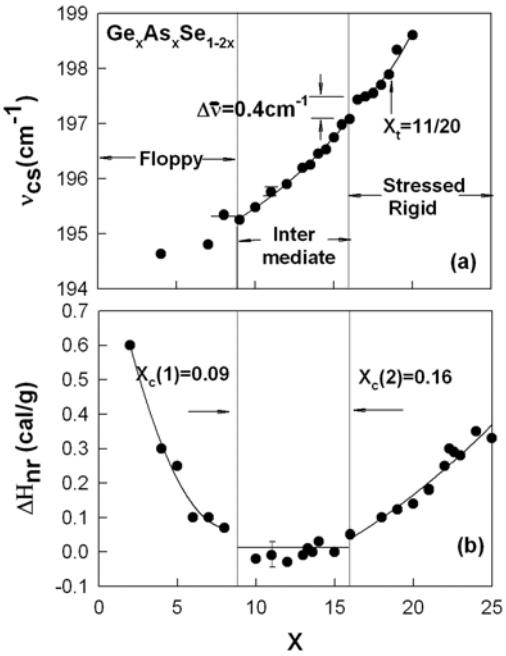

Fig. 7. Variation in the corner sharing mode frequency , υ_{CS}, and the non-reversing heat flow term, $\Delta H_{nr}(x)$ in ternary $Ge_xAs_xSe_{1-2x}$ glasses displaying three distinct regime in x that coincide. The two thresholds, one at $x = X_c(1) = 9\%$ and the second at $x = X_c(2) = 16\%$ represent the rigidity and stress transitions. The interval between these transitions represents the intermediate phase, which coincides with the reversibility window.

boundaries in the ternary glass system. The reversibility window onbserved here is one of the widest reported to date. In the intervening region, $r_1 < r < r_2$, one has a network that is rigid but unstressed. By plotting the mode frequency squared, υ^2, serving as a measure of Raman optical elasticity, one can extract the underlying elastic power-laws, "p", using equation (12).

$$\upsilon^2 - \upsilon_c^2 = A\,(r - r_c)^p \qquad (12)$$

In equation (12), υ_c and r_c represent respectively the frequency and the mean coordination number at the elastic threshold composition. Analysis of the Raman data gives a value of the power-law, p = 1.04 (3) in the IP, and a value of p = 1.52 (5) in stressed-rigid phase of the present ternary. Parallel results have been found in many other glass systems with nearly the same power-laws in the IP and the stressed-rigid phase. Numerical simulations [5, 59] of amorphous systems modeled as random networks predict [5,59] a power law p = 1.4 in the stressed-rigid phase , in fair agreement with the experiments. There are currently no theoretical prediction of the elastic power-law in the IP to compare the observed value of p = 1.4(3). The consistency of Raman elastic power-laws in several covalent glasses is reassuring. These results are suggestive of common underlying principles that control elastic behavior of networks in these domains in general. But there are some caveats in using Raman scattering as a probe of elastic behavior of glasses. When networks are demixed instead of fully polymerized, or when Raman vibra- -tional modes are broad and not well resolved, use of the technique to decode elastic phases is then compromised. Furthermore, vibrational modes that reside in the flexible part of a network or a decoupled monomeric unit of a glass network, cannot be expected to serve as a viable probe of network elastic behavior.

3.3 Electrical conductivity

Traditional solid electrolytes such as AgI, Ag_2Se, Ag_2S as additives in base oxide and chalcogenide glasses such as $AgPO_3$, As_2S_3 form a class of materials known as solid electrolyte glasses [60-63]. Recent work [60, 64, 65] on these systems has also shown that the Ag based traditional solid electrolytes can also exist in a glassy phase as additives in chalcogenide glasses. These materials have attracted much attention because their ionic conductivity increases remarkably as the solid electrolyte additive content of the glasses increases [61, 62, 66-68]. The origin of fast-ion conduction in these systems has been a subject ongoing debate with some emphasizing the decoupling of fast ion transport from structural relaxation [69-72], while others emphasizing the close connection between glass structure and ion transport [73]. One particular solid electrolyte glass system that has received particular attention is the $(AgPO_3)_{1-x}(AgI)_x$ system. It has been investigated by more than a dozen research groups [63, 66, 67, 74-76] in a wide variety of experiments [63, 67, 74, 77]. Recently Novita et al. found that the T_g of the base glass ($AgPO_3$) in its dry state (T_g = 254°C) is substantially higher than in its wet state (T_g ~ 181°C) [61, 78]. Furthermore, non-reversing enthalpy at Tg of dry samples are characteristic of stressed-rigid elastic networks while those of wet samples synthesized at laboratory ambient environment are characteristic of flexible networks[43]. By alloying AgI in very dry $AgPO_3$ base glass, one observes the reversibility window in the 9.5% < x < 37.8% range (set A) [61] as illustrated in Fig. 8. For a base glass

that was slightly less dry (set B) [78], the RW decreased substantially in width as illustrated by the blue data set in Fig. 8. Variation of electrical conductivity in the dry set of samples shown in the lower panel of Fig. 8 reveals steps at the two elastic phase boundaries. At x > 37.8% glass

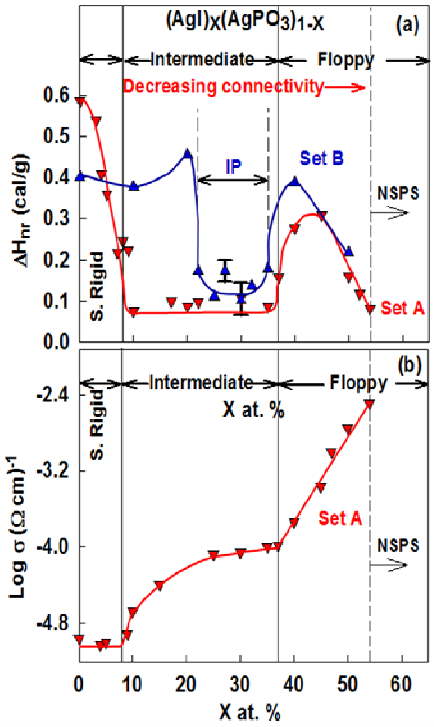

Fig. 8. Variation of the (a) non-reversing enthalpy at Tg and (b) electrical conductivity in very dry $(AgPO_3)_{1-x}(AgI)_x$ glasses (set A) showing a close connection between the three elastic phases and fast-ion conduction.For the less dry set of samples B, the reversibility window decreases significantly illustrating the need to work with rather dry samples to observe the intrinsic physical behavior of these electrolyte glasses. Figure taken from ref. Novita et al. [78].

networks become elastically flexible and the ionic conductivity is found to increase logarithmically [61] with a power-law,

$$\sigma = \sigma_o (x - x_c)^t \qquad (13)$$

t = 1.78. In equation (13), x_c represents the conductivity threshold of 37.8%.

What are the implications of these results on fast-ion conduction in glasses? The central message of Fig. 8 and the power-law variation is that fast-ion conduction is closely tied to the elastic nature of underlying glassy backbones [61, 78]. Ag^+ ion mobilities are apparently facilitated when elastic energy to displace neighbouring ions is small as it will be in the flexible phase of these glasses. These conductive pathways apparently form even in the IP, which is marginally rigid. The power-law variation of conductivity in the flexible phase of t = 1.78, percolation theory suggests [79], is signature of filamentary conductive pathways in a 3D network that connect as x exceeds 37.8%, leading to the giant enhancement of conductivity. Evidence for such conductive pathways has been obtained directly at x = 50% in field emission experiments on mesoscale wires of the present solid electrolyte.

The absence of steplike variation of electrical conductivity with AgI content [61, 78] in previous work in the field is easily reconciled within the present findings. In these earlier reports the base glass used in the experiments possessed a T_g of about 180°C, characteristic of wet samples that are known to form elastically flexible networks [66, 67]. Alloying AgI in such networks will not display the elastic phases transitions since the role of the additive is to drive the base network even more elastically flexible [66, 67]. To observe the intrinsic variation of conductivity in these systems there is a need to synthesize dry samples and suppress extrinsic effects [43, 78]. In Chapter 2 , Malki et al. dwell on these issues more extensively and the interested reader is steered to the discussion there. We conclude this section with two comments. The observation of reversibility windows in solid electrolyte glasses is of profound interest. In these glassy systems, ion valences are not satisfied locally, and estimates of mechanical network constraints are not obvious as they were in covalent systems. The observation of RWs suggests that classification of glasses in terms of the threeelastic phases is a more general phenomenon [22]. It is not confined to covalent glasses. Recently a joint theoretical and experimental study has provided evidence of an electronic signature of the IP in binary Ge_xSe_{1-x} glasses [80]. The experimental probe used extended X-ray absorption fine structure analysis near the absorption edges-XANES and details of these experiments appear in a chapter in the present volume.

4. Global elastic phase diagrams

In glass science one often identifies regions of glass formation with the help of composition triangles, as summarized in the excellent book of Borisova [32]. It is instructive to map the three elastic phases observed in covalent glasses onto their glass forming compositions and construct global elastic phase diagrams. Such phase diagrams are illustrated for the case of the Ge-As-Se and Ge-P-Se ternaries in Fig. 9 and 10 espectively. The

flexible elastic phase is generally formed in Se-rich glasses (lower left corner), which consist of polymeric Se_n chains that are intrinsically flexible, possessing one floppy mode per atom [6, 8]. Moving away from that Se corner either towards Ge or As, the polymeric Se_n chains become progressively cross-linked as IPs are manifested in a narrow but well defined range of compositions indicated by the green hashed marked regions. With a further increas in cross-linking, networks become over-constrained, and stressed-rigid elastic phases appear. Glass compositions in the latter phase, especially along the binary compositions, Ge-Se or As-Se usually nanoscale phase separate, and display a threshold behavior of T_gs [49, 81]. Such compositions are highlighted in a brick red color in these figures. On the other hand ternary selenides and sulfides containing equal proportions of Ge and As (or P) usually form homogeneously crosslinked networks extending

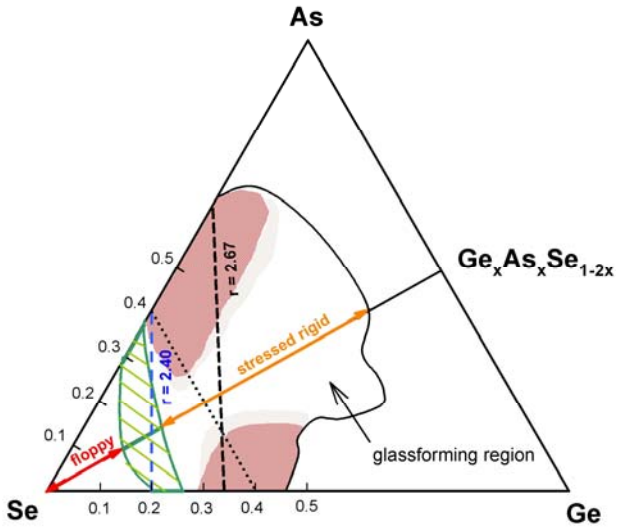

Fig. 9. Glass forming region and elastic phases in the Ge-As-Se ternary. The figure is taken from ref. Tao Qu et al. [20] The green hashed marked region identifies the IP in the ternary. The brick colored regions represent glasses that are nanoscale phase separated.

to mean coordination number $\boldsymbol{r} \sim 3$. In these particular glasses, $T_g(\boldsymbol{r})$ increase monotonically with $\boldsymbol{r}$ – a signature of networks that are nearly fully polymerized, and these systems are ideal to probe [82] the elastic phase transitions of interest here.

The global elastic phase diagrams also serve to illustrate that RWs are often limited to compositions where networks are reasonably well

polymerized. In covalent systems, RWs are unlikely to extend to compositions where network character is lost as demixing or nsps occurs. A case in point is the P-Se binary where glass compositions at x > 40% become intrinsically demixed as P_4Se_3 molecular cages decouple from the backbone. Not surprisingly, RWs extend only to about 40% of P along the P-Se binary. A parallel circumstance apparently prevails in the As-Se binary glass system. On the other hand, for ternary glasses containing equal proportions of Ge and P(or As) for example, experiments reveal IPs to extend to $\boldsymbol{r} \sim 2.48$ as depicted in Figs. 9 and 10.

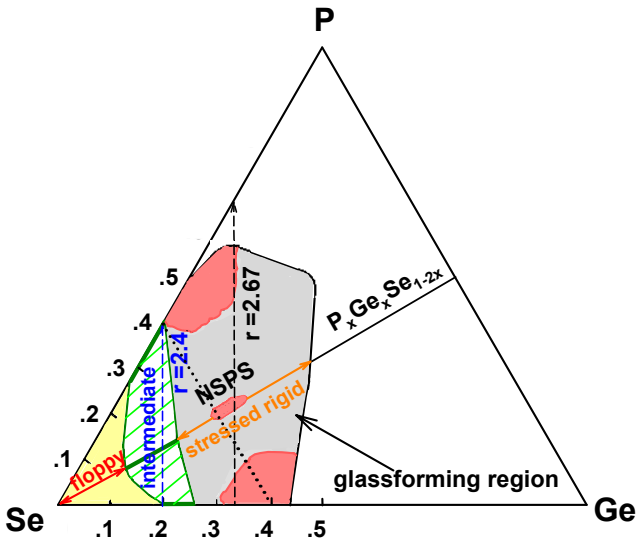

Fig. 10. Glass forming region and elastic phases in the Ge-P-Se ternary. The figure is taken from ref. S. Chakravarty et al. [18] The green hashed marked region identifies the IP in the ternary. The brick colored regions represent glasses that are nanoscale phase separated.

5. Intermediate phases and glass structure

The discovery of IPs in a variety of glass systems has stimulated interest in modeling their structures. It is natural to inquire, what aspects of network structure control their widths and centroids? Given the fairly complete nature of results on the chalcogenides (Fig. 6) now available, it is possible to identify several generic features of these data that can serve as bounds for any structural model that is developed to model these phases.

Some of these generic features are as follows.

(1) The group IV(Si, Ge) selenides display IPs that exist in the 2.40 < ***r*** < 2.52 range, with the Si-Se binary displaying a somewhat larger width than the Ge-Se one.

(2) The group V(As, P) selenides show IPs to exist in the 2.28 < r < 2.40 range , i.e., shifted to lower ***r*** in relation to the Group IV selenides.

(3) In ternary selenides comprising of equal proportions of group IV and group V elements, IPs span a region of ***r***-space that encompasses IPs of corresponding binary glasses. For example, IP of the $Ge_xAs_xSe_{1-2x}$ ternary covers a range of ***r***-space, 2.28 < ***r*** < 2.48, which includes IPs of the corresponding binary glasses, As_xSe_{1-x} (2.28 < ***r*** < 2.40) and Ge_xSe_{1-x} (2.40 < ***r*** < 2.52).

(4) In ternary sulfides containing equal proportions of group IV and group V elements, IPs possess smaller widths than their selenide counterparts, although their centroids appear to be nearly the same.

(5) In binary P_xS_{1-x} glasses, the IP is shifted to an anomalously low connectivity, 2.14 < r < 2.19.

(6) Finally, in binary As_xS_{1-x} glasses, the IP resides in the 2.23 < ***r*** < 2.30 range, residing almost half way in between the IPs of the As-Se and the P-S binaries.

There have been several recent efforts to build structural models of binary As-Se and Ge-Se glasses using ab-initio molecular dynamics simulations [83-88]. These approaches typically model a network composed of 120 atoms. Neutron structure factors along with partial pair distribution functions in conjunction with MD are used to develop structural models of these glasses. C. Massobrio et al. [88] have recently built and compared models of $SiSe_4$ with $GeSe_4$ glass to obtain concentrations of the two structural motifs, CS and ES tetrahedra, and correlate these with IP widths in these binaries. Even with excellent fits to neutron structure factors, the recognition has emerged in recent years that a substantial concentration of non 8-N conforming local coordinations persist in such models. These high-T defect configurations frozen could be due to the high quench rates used in preparing these glasses in MD. In spite of these caveats, ingenious schemes are being developed to offset some of these limitations. To increase the size of models, J. Mauro and Varsheneya used an ab-initio approach to obtain potentials that would describe atomic interactions for the case of the Ge-Se and As-Se binary glasses. They then proceeded to build larger models of these glasses containing 10, 000 atoms, and from a vibrational analysis found evidence [85, 86] of the mean field rigidity transition near ***r*** ~ 2.40 in their models of these glasses. An interesting aspect of their model for As-Se glasses is that they found evidence for the presence of of both PYR and QT As local structures in harmony with experiments [17].

Our approach here is to connect the experimental data on IPs to structural chemistry of glasses and their glass forming tendency. IPs are

manifested in networks that are predominantly composed of local structures that are isostatic. We use mean-field constraint counting algorithms to estimate the count of constraints of specific local structures. In a 3D network, for an atom possessing a coordination number ***r*** (2 or greater), one associates ***r***/2 bond stretching constraints, and 2***r*** - 3 bond bending ones. A dangling end [89] possessing ***r*** = 1, contributes ½ of a bond-stretching constraints but no bond-bending constraint. Based on these rules, we can identify 4 distinct local structures (Fig. 11) that are isostatic, i.e., possess 3 constraints/atom, and include, group V atom centered (i) *pyramidal* (PYR) and (ii) *quasi tetrahedral* (QT) units, and group IV centered (iii) *corner-sharing* (CS) and (iv) *edge-sharing* (ES) tetrahedral units. The term "structural variance" was first used by Sartbeva et al. [90] to denote the variable length of Se_n chain-like links connecting tetrahedral units in binary Ge_xSe_{1-x} glasses modeled using depleted amorphous Si networks. In the present work we use the term "structural variance" to reflect the variability of these 4 possible local structures (fig. 11), which are formed systematically as glass stoichiometry or connectivity ***r*** is varied. In our view, population of at least two or more isostatic local structures is essential for an IP to be manifested in real glasses. A monolithic network composed exclusively of just one type of a local structure may not be sufficient to provide the entropy needed to stabilize IPs.

Feature (1) reveals the IP in the two group IV- selenides to onset at $r_1 = 2.40(1)$, and to terminate at $r_2 = 2.50(1)$ in the case of the Ge-Se binary, but to a slightly larger value of $r_2 = 2.54(1)$ in the case of the Si-Se binary. Here the two local structures that provide structural variance in the IP include Si or Ge centered CS and ES tetrahedra (see Fig. 11). The chemical stoichiometry of infinitely long ES tetrahedral chains corresponds to a mean coordination number of r = 2.67. We believe the extension of the IP to r > 2.40 is due to the presence of ES local structures in addition to CS ones present in these glasses. These ideas are in spirit similar to the Size Increasing Cluster Approximation (SICA) developed by Micoulaut and Phillips [55]. They used constraint counting algorithms on clusters to show that the upper phase boundary is tied to the fraction ES units that agglomerate with CS ones in these group IV selenides.

Feature (2) relates to the case of group V (As, P) selenides in which IPs exist at r < 2.40. Here the two local structures of relevance include QT and PYR units (Fig. 11). The onset of the IP near r = 2.28 would be in harmony with the stoichiometry of the QT units, while the end of the IP near r = 2.40 is consistent with the. stoichiometry of PYR units. The general picture here is that as As or P is steadily alloyed in a base Se glass, QT units grow in concentration to acquire a global maximum near ***r*** = 2.28 , and at a slightly higher concentration, PYR units globally maximize in concentration near ***r*** = 2.40. The QT local structures pack better than PYR ones and their presence in IPs is expected given their space filling nature Although spectroscopic (Raman [91] and NMR [91]) evidence of these two local

structures is unambiguous in binary P-Se glasses [91], at present such is not the case in the As-Se binary system. The latter is an issue of ongoing investigations.

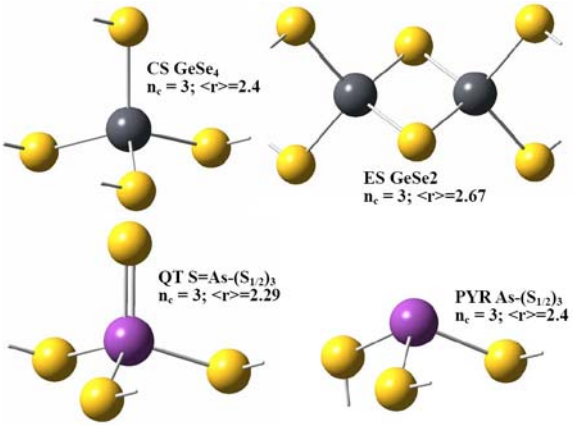

Fig. 11. Local structures of interest in IPs of chalcogenide glasses. Ge based corner sharing (top right) and edge-sharing tetrahedral units(top left) , and As based quasi-tetrahedral (bottom left) and pyramidal (bottom right). The mean coordination number, and count of constraints/atom for these structures are also indicated for each unit.

Feature (3) readily follows if the structural variance contributing to features (1) and (2) are accepted as described above. In the $Ge_xAs_xSe_{1-2x}$ ternary one expects all 4 local structures of Fig. 11 to be manifested, and to contribute towards forming the stress-free backbone of the IP. Raman spectroscopy evidence largely supports the contention. The onset of the IP at $\boldsymbol{r}$ = 2.27 and its end near $\boldsymbol{r}$ = 2.48, would be consistent with local structures evolving in the following sequence as a function of increasing $\boldsymbol{r}$; QT units, followed by PYR units and CS units, followed by ES units. In the corresponding $Ge_xP_xSe_{1-2x}$ ternary (Fig. 6) the IP resides in the $2.30 < \boldsymbol{r} < 2.43$ range. Why is the width of the IP in $Ge_xP_xSe_{1-2x}$ ternary smaller than the one in the $Ge_xAs_xSe_{1-2x}$ ternary? In the Ge-P-Se ternary, it is well established [18] from spectroscopic and thermal measurements that with increasing P content, and particularly near $\boldsymbol{r}$ = 2.40, some of the P begins to demix from the backbone in the form of P_4Se_3 molecules. We believe the smaller width of the IP in the Ge-P-Se ternary relative to the Ge-As-Se one, results due to some loss of connective tissue as P begins to partially demix from the backbone, thus shifting down in r-space the upper end of the IP.

Feature (4) reveals that IP-width of ternary sulfides (such as $Ge_xAs_xS_{1-2x}$, $\Delta r = 0.12$) to be smaller (fig. 6) than the IP-width in corresponding selenides (such as $Ge_xAs_xSe_{1-2x}$, $\Delta r = 0.21$). What aspect of structure contributes to this feature? We believe that there are two characteristic of the sulfides that come into play here, one (a) the tendency of pure S to crystallize as a molecular crystal composed of S_8 rings rather than form polymeric chains as in the case of the selenides, and second (b) binary As-sulfides such as As_4S_3 and As_4S_4, which form molecular cages rather than polymeric structures, demixing from backbones as the As and Ge concentration approaches approximately 13% [92]. Demixing of these molecular species at the low end and at the high end of the IP, limits the range of ***r*** across which a backbone structure can prevail. The natural consequence is a shift of the low end of the IP up and of the high end of the IP down resulting in a narrowing of the IP-width in the sulfides in relation to the selenides.

Features (5) and (6) relate to the IP of the P-S and As-S binary glasses. These are particularly fascinating results because they stand out from the rest of the IP data shown in Fig. 6. The shift of the IP in P-S binary glasses to a low value of r can be traced to complete demixing [53, 54] of the excess S from the backbone, which comprises of P-centered PYR and QT units. In the IP, Raman scattering data shows excess S to be present in a S_n chain form and not as S_8 rings. The chemical stoichiometry of the IP backbone in P-S glasses under that circumstance is found to be identical to that of P-Se glasses at the center of the IP. *These data suggest that IP centroids provide a measure of network polymerization*, with P-Se glasses and P-S glasses representing the two extremes; the former binary is an example of system where the excess Se forms part of the backbone, while the latter is an example where the excess S is completely decoupled from the IP backbone. Given that finding, the IP centroid in the As-S binary appears to represent an intermediate case, i.e., a case where about half of the excess S forms part of the backbone, while the other half appears to be decoupled from it. These ideas when put in context with other findings, such as those on variation of T_g, molar volumes and the boson mode scattering strength with glass composition provide a fairly comprehensive picture [53, 54] of these important photonic materials as composed of partially polymerized network glasses.

6. Broader perspectives

We conclude with some general remarks bearing on the broader implications of the discovery of IPs in glass science.

6.1 Intermediate Phases in amorphous covalent thin-films

In the review we have focused on using melt quenched bulk alloy glasses as test systems to probe elastic phases. These materials can be synthesized in not only a pure, dry and homogeneous form but also probed in diffraction, thermal, optical and nuclear methods with relative ease. IPs are also observed in amorphous thin-films of these systems with rather profound consequences on their functionality. Control of thin-film stoichiometry and structure relaxation poses challenges in synthesis of these systems. The discovery of giant photo-contraction (PC) of obliquely deposited amorphous Ge_xSe_{1-x} thin- films [25] in the early 1980s was

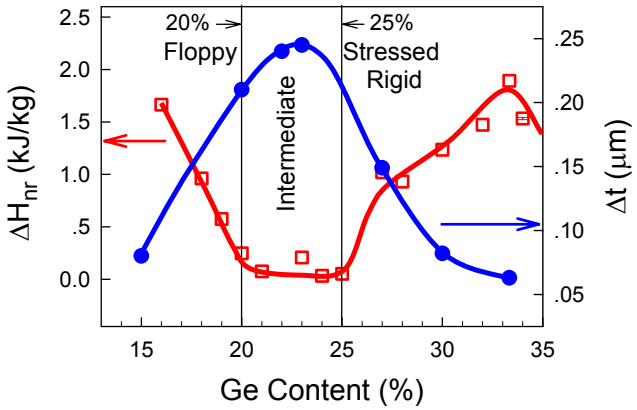

Fig. 12. Thickness changes of obliquely deposited Ge_xSe_{1-x} thin films after Hg-Xe vapor lamp illumination (●) showing a bell shaped curve with a broad maximum in the IP. The non-reversing enthalpy at T_g of corresponding bulk glasses (ΔH_{nr} □) reveals a global minimum in the 20% < x < 25% range identified as the Intermediate phase. See text for details.Figure taken from ref.[25].

recently revisited [25]. And it has emerged that the PC effect is maximized [25] in IP compositions as illustrated in Fig. 12. These new results complemented by Raman optical characterization of thin-films have yielded insights into the microscopic origin of the giant PC effect. These new results show that columns of the porous films consist of nanometric sized composite filaments. The maximum of the PC effect can be traced to the photomelting of stress-free columns of nominally $Ge_{25}Se_{75}$ stoichiometry in the IP. At x > 25%, suppression of the PC effect arises due to growth of a photo-inactive stressed rigid Ge-rich phase (approx Ge_2Se_3 stoichiometry) that grows in the inter-columnar space. Pair-producing radiation leads to photo reconstruction of the stress-free columns with the Ge-rich phase. At x < 20%, films grow with columns becoming increasingly Se-rich and thus stressed, leading to reduced photomelting [25] .It is likely that investigations of amorphous thin-

films residing in IP compositions in future may reveal new functionalities for applications in devices.

6.2 Intermediate Phases in oxides and H-bonded systems

Discovery of IPs in chalcogenide glasses has stimulated interest in searching for such phases in other than covalent systems, such as oxides, solid electrolytes, and H-bonded systems such as sugars and alcohols. IPs have now been observed in alkali-silicates [93] and alkali-germanates [31] . The case of a AgI based solid electrolyte [78] system was briefly touched upon in the present review. Calorimetric measurements on glassy trehalose have recently revealed [22] that the non-reversing enthalpy at T_g is vanishing, suggesting that the disaccharide is most likely an example of a self-organized structure and the bioprotective functionality a consequence of it. These new observations suggest that classification of glassy networks into 3 generic elastic phases is apparently not confined to covalent systems but may well be generic to the disordered state of matter.

6.3 Intermediate Phases and Protein folding

The discovery of IPs continues to have important consequences in understanding protein functionality. Close analogies in the elastic behavior of glassy networks with proteins were recognized by M.F.Thorpe [94]. Proteins also display *three* states that are elastically similar to the ones observed in network glasses. The *native-, transition- and folded-* states in proteins have been compared to the *stressed-rigid*, *intermediate* and *flexible* phases of network glasses. In recent work Kister and Phillips [95] have emphasized the importance of hydrophobicity scales in understanding protein-protein interactions which are mediated by water. They have applied their approach to two simple proteins, and have shown that only 12% of the amino acids encode protein functionality.

6.4 Intermediate Phases at Semiconductor interfaces

The notion of self-organization at semiconductor interfaces was recognized and demonstrated for thin-film transistors [96] used in liquid crystal displays by Lucovsky and Phillips. In these transistors a thin film of amorphous Si:N:H gate dielectric is used. By systematically tuning the ratio $R = NH_3/SiH_4$ in the range $2 < R < 15$, they found that electron mobilities to display their highest values near $R \sim 10.0(5)$ corresponding to the IP observed here in a 2D structure. These ideas have proved to be central to developing functional high K (dielectric constant) CMOS devices using HfO_2 as the dielectric. In these CMOS devices, two monolayers of a Si suboxide is grown over Si, before depositing the high K dielectric. The Si-

suboxide serves as a self-organized buffer layer, and shields the active channel in Si from being exposed to defects formed at the HfO_2/SiO_2 interface. This 45 nm technology was recently announced by Intel Corp [97]. Basic ideas on self-organization of disordered networks have thus had visible consequences in moving along the Semiconductor road map.

6.5 Multiscale structural self-organization in soft condensed matter

A common thread linking diverse systems such as, transition metal oxides [98] (High Temperature oxide superconductors, Colossal Magneto-Resistive Maganites), conjugated organic polymers [99] and Biological macro-molecules [100] (DNA) is the interplay between short-range forces that serve as constraints, and long-range ones that stabilize different macroscopic structures. Bishop and collaborators at Los Alamos National Laboratory have emphasized [101] the role of these basic interactions operative on different length scales, which lead to phase diagrams that bear a striking resemblance to the ones we have encountered in glasses.

In summary, self-organization effects in complex systems appear to be manifested across several disciplines including soft condensed matter, electrical engineering, protein science, and computer science. And as we reflect on these ideas, we are reminded of the words [102] of Oliver Wendell Holmes Sr., "*Every now and then a person's mind is stretched by a new idea or sensation, and never shrinks back to its former dimensions*

Acknowledgements

It is a pleasure to acknowledge discussions with a number of colleagues over the years on issues relating to Intermediate Phases and flexibility/rigidity of networks, and some of these include Professor J.C. Phillips, Professor M. Micoulaut, Professor M.F. Thorpe, Professor M. Mitkova, Professor Richard Kerner, Professor Darl McDaniel, Professor G. Lucovsky and Dr A. Bishop. The present work is supported by the US National Science Foundation grant DMR-04 -56472.

References

[1] J. C. Phillips, J. Non-Cryst. Solids **34**, 153 (1979).
[2] M. F. Thorpe, J. Non-Cryst. Solids **57**, 355 (1983).
[3] J. L. Lagrange, Mecanique Analytique (Desaint, Paris, 1788).
[4] J. C. Maxwell, Philos. Mag. **27**, 294 (1864).
[5] H. He, M. F. Thorpe, Phys. Rev. Lett. **54**, 2107 (1985).

[6] P. Boolchand, R. N. Enzweiler, R. L. Cappelletti, W. A. Kamitakahara, Y. Cai, M. F. Thorpe, Solid State Ionics **39**, 81 (1990).
[7] P. Boolchand, W. Bresser, M. Zhang, Y. Wu, J. Wells, R. N. Enzweiler, J. Non-Cryst. Solids **182**, 143 (1995).
[8] W. A. Kamitakahara, R. L. Cappelletti, P. Boolchand, B. Halfpap, F. Gompf, D. A. Neumann, H. Mutka, Phys. Rev. B **44**, 94 (1991).
[9] D. Selvanathan, W. J. Bresser, P. Boolchand, Phys. Rev. B **61**, 15061 (2000).
[10] P. Boolchand, X. Feng, W. J. Bresser, J. Non-Cryst. Solids **293**, 348 (2001).
[11] D. Selvanathan, W. J. Bresser, P. Boolchand, B. Goodman, Solid State Commun. **111**, 619 (1999).
[12] P. Boolchand, D. G. Georgiev, B. Goodman, J. Optoelectron. Adv. Mater. **3**, 703 (2001).
[13] M. F. Thorpe, D. J. Jacobs, M. V. Chubynsky, J. C. Phillips, J. Non-Cryst. Solids **266**, 859 (2000).
[14] M. F. Thorpe, M. V. Chubynsky, in Phase Transitions and Self-organization in Electronic and Molecular Networks, edited by J. C. Phillips and M. F. Thorpe (Kluwer Academic/Plenum Publishers, New York, 2001), p. 43.
[15] F. Wang, S. Mamedov, P. Boolchand, B. Goodman, M. Chandrasekhar, Phys. Rev. B **71**, 174201 (2005).
[16] P. Boolchand, G. Lucovsky, J. C. Phillips, M. F. Thorpe, Phil. Mag. **85**, 3823 (2005).
[17] D. G. Georgiev, P. Boolchand, M. Micoulaut, Phys. Rev. B **62**, R9228 (2000).
[18] S. Chakravarty, D. G. Georgiev, P. Boolchand, M. Micoulaut, J. Phys. Condens. Matter **17**, L1 (2005).
[19] P. Boolchand, M. Jin, D. I. Novita, S. Chakravarty, J. Raman Spectrosc. **38**, 660 (2007).
[20] T. Qu, D. G. Georgiev, P. Boolchand, M. Micoulaut, in Supercooled Liquids, Glass Transition and Bulk Metallic Glasses, edited by T. Egami, A. L. Greer, A. Inoue and S. Ranganathan (Materials Research Society, 2003), Vol. 754, p. 157.
[21] U. Vempati, P. Boolchand, J. Phys. Condens. Matter **16**, S5121 (2004).
[22] P. Boolchand, M. Micoulaut, P. Chen, in Phase Change Materials: Science and Applications, edited by S. Raoux and M. Wuttig (Springer, Heidelberg, 2008), p. 37.
[23] P. Boolchand, D. G. Georgiev, M. Micoulaut, J. Optoelectron. Adv. Mater. **4**, 823 (2002).
[24] W. H. Zachariasen, J. Am. Chem. Soc. **54**, 3841 (1932).
[25] M. Jin, P. Chen, P. Boolchand, S. Rajagopalan, K. L. Chopra, K. Starbova, N. Starbov, Phy. Rev. B, arXiv:0808.3289v1 (Accepted).
[26] G. Adam, J. H. Gibbs, J. Chem. Phys. **43**, 139 (1965).
[27] L. M. Martinez, C. A. Angell, Nature **410**, 663 (2001).

[28] A. Widmer-Cooper, H. Perry, P. Harrowell, D. R. Reichman, Nat Phys **4**, 711 (2008).
[29] M. Reading, B. K. Hahn, B. S. Crowe, US Patent 5224775 (1993).
[30] P. G. Debenedetti, F. H. Stillinger, Nature **410**, 259 (2001).
[31] K. Rompicharla, D. I. Novita, P. Chen, P. Boolchand, M. Micoulaut, W. Huff, J. Phys.: Condens. Matter **20**, 202101 (2008).
[32] Z. U. Borisova, Glassy semiconductors (Plenum Press, New York, 1981).
[33] T. Franosch, W. Gotze, J. Phys.: Condens. Matter **6**, 4807 (1994).
[34] L. Berthier, G. Biroli, J. P. Bouchaud, L. Cipelletti, D. E. Masri, D. L'Hote, F. Ladieu, M. Pierno, Science **310**, 1797 (2005).
[35] R. Böhmer, C. A. Angell, Phys. Rev. B **45**, 10091 (1992).
[36] P. W. Anderson, Science **267**, 1615 (1995).
[37] C. A. Angell, in Insulating and Semiconducting Glasses, edited by P. Boolchand (World Scientific, Singapore; River Edge, NJ, 2000), p. 1.
[38] M. Reading, D. Elliott, V. Hill, J. Therm. Anal. Calorim. **40**, 949 (1993).
[39] L. C. Cai, P. Boolchand, Phil. Mag. B **82**, 1649 (2002).
[40] A. DeGusseme, L. Carpentier, J. F. Willart, M. Descamps, J. Phys. Chem. B **107**, 10879 (2003).
[41] N. O. Birge, S. R. Nagel, Phys. Rev. Lett. **54**, 2674 (1985).
[42] P. K. Dixon, S. R. Nagel, Phys. Rev. Lett. **61**, 341 (1988).
[43] D. I. Novita, P. Boolchand, Phys. Rev. B **76**, 184205 (2007).
[44] J. H. Gibbs, E. A. DiMarzio, J. Chem. Phys. **28**, 373 (1958).
[45] S. Mahadevan, A. Giridhar, J. Non-Cryst. Solids **143**, 52 (1992).
[46] G. G. Naumis, Phys. Rev. B **73**, 172202 (2006).
[47] R. Kerner, M. Micoulaut, J. Non-Cryst. Solids **210**, 298 (1997).
[48] P. Chen, Ph.D. Thesis, University of Cincinnati (2009).
[49] P. Boolchand, P. Chen, M. Jin, B. Goodman, W. J. Bresser, Physica B-Condensed Matter **389**, 18 (2007).
[50] P. Boolchand, W. J. Bresser, Phil. Mag. B **80**, 1757 (2000).
[51] L. Tichý, H. Tichá, J. Non-Cryst. Solids **189**, 141 (1995).
[52] L. Pauling, The Nature of the Chemical Bond (Cornell University, Ithaca, NY, 1960).
[53] P. Boolchand, P. Chen, U. Vempati, J. Non-Cryst. Solids, arXiv:0809.1469v2 (accepted).
[54] P. Chen, C. Holbrook, P. Boolchand, D. G. Georgiev, K. A. Jackson, M. Micoulaut, Phys. Rev. B, arXiv:0810.3637v1 (Submitted).
[55] M. Micoulaut, J. C. Phillips, Phys. Rev. B **67**, 104204 (2003).
[56] J. Gump, I. Finkler, H. Xia, R. Sooryakumar, W. J. Bresser, P. Boolchand, Phys. Rev. Lett. **92**, 245501 (2004).
[57] X. W. Feng, W. J. Bresser, P. Boolchand, Phys. Rev. Lett. **78**, 4422 (1997).

[58] M. Micoulaut, J. C. Phillips, J. Non-Cryst. Solids **353**, 1732 (2007).
[59] D. S. Franzblau, J. Tersoff, Phys. Rev. Lett. **68**, 2172 (1992).
[60] P. Boolchand, W. J. Bresser, Nature **410**, 1070 (2001).
[61] D. I. Novita, P. Boolchand, M. Malki, M. Micoulaut, Phys. Rev. Lett. **98**, 195501 (2007).
[62] C. Holbrook, P. Chen, D. I. Novita, P. Boolchand, IEEE Transactions on Nanotechnology **6**, 530 (2007).
[63] C. A. Angell, Annu. Rev. Phys. Chem. **43**, 693 (1992).
[64] M. Mitkova, Y. Wang, P. Boolchand, Phys. Rev. Lett. **83**, 3848 (1999).
[65] Y. Wang, M. Mitkova, D. G. Georgiev, S. Mamedov, P. Boolchand, J. Phys. Condens. Matter **15**, S1573 (2003).
[66] D. L. Sidebottom, Phys. Rev. B **61**, 14507 (2000).
[67] M. Mangion, G. P. Johari, Phys. Rev. B **36**, 8845 (1987).
[68] E. A. Kazakova, Z. U. Borisova, Fiz. Khim.Stekla **6**, 424 (1980).
[69] M. D. Ingram, Phys. Chem. Glasses **28**, 215 (1987).
[70] F. S. Howell, R. A. Bose, P. B. Macedo, C. T. Moynihan, J. Phys. Chem. **78**, 639 (1974).
[71] C. A. Angell, Solid State Ionics **18-9**, 72 (1986).
[72] G. N. Greaves, K. L. Ngai, J. Non-Cryst. Solids **172**, 1378 (1994).
[73] M. D. Ingram, C. T. Imrie, J. Ledru, J. M. Hutchinson, J. Phys. Chem. B **112**, 859 (2008).
[74] J. D. Wicks, L. Borjesson, G. Bushnellwye, W. S. Howells, R. L. McGreevy, Phys. Rev. Lett. **74**, 726 (1995).
[75] E. Kartini, M. F. Collins, T. Priyanto, M. Yusuf, N. Indayaningsih, E. C. Svensson, S. J. Kennedy, Phys. Rev. B **61**, 1036 (2000).
[76] T. Minami, J. Non-Cryst. Solids **73**, 273 (1985).
[77] E. Kartini, M. F. Collins, T. Priyanto, M. Yusuf, N. Indayaningsih, E. C. Svensson, S. J. Kennedy, Phys. Rev. B **61**, 1036 (2000).
[78] D. I. Novita, P. Boolchand, M. Malki, M. Micoulaut, Phys. Rev. B, arXiv:0808.1154v1 (Submitted).
[79] R. Zallen, The Physics of Amorphous Solids (Wiley, New York, 1983).
[80] F. Inam, G. Chen, D. N. Tafen, D. A. Drabold, arXiv:0806.1039v1 (2008).
[81] P. Boolchand, Asian J. of Phys. **9**, 709 (2000).
[82] P. Boolchand, D. G. Georgiev, T. Qu, F. Wang, L. C. Cai, S. Chakravarty, Comptes Rendus Chimie **5**, 713 (2002).
[83] M. Cobb, D. A. Drabold, R. L. Cappelletti, Phys. Rev. B **54**, 12162 (1996).
[84] F. Inam, M. T. Shatnawi, D. Tafen, S. J. L. Billinge, P. Chen, D. A. Drabold, J. Phys.: Condens. Matter **19**, 455206 (2007).
[85] J. C. Mauro, A. K. Varshneya, J. Non-Cryst. Solids **353**, 1226 (2007).
[86] J. C. Mauro, A. K. Varshneya, J. Am. Ceram. Soc. **90**, 192 (2007).
[87] M. A. Brière, M. V. Chubynsky, N. Mousseau, Phys. Rev. E **75**,

056108 (2007).
[88] C. Massobrio, M. Celino, A. Pasquarello, J. Phys. Condens. Matter **15**, S1537 (2003).
[89] P. Boolchand, M. F. Thorpe, Phys. Rev. B **50**, 10366 (1994).
[90] A. Sartbaeva, S. A. Wells, A. Huerta, M. F. Thorpe, Phys. Rev. B **75**, 224204 (2007).
[91] D. G. Georgiev, P. Boolchand, H. Eckert, M. Micoulaut, K. Jackson, Europhys. Lett. **62**, 49 (2003).
[92] T. Qu, P. Boolchand, Phil. Mag. **85**, 875 (2005).
[93] Y. Vaills, T. Qu, M. Micoulaut, F. Chaimbault, P. Boolchand, J. Phys. Condens. Matter **17**, 4889 (2005).
[94] A. J. Rader, B. M. Hespenheide, L. A. Kuhn, M. F. Thorpe, Proceedings of the National Academy of Sciences of the United States of America **99**, 3540 (2002).
[95] A. E. Kister, J. C. Phillips, Proceedings of the National Academy of Sciences of the United States of America (arXiv:0803.2644) (submitted).
[96] G. Lucovsky, D. A. Baker, M. A. Paesler, J. C. Phillips, J. Non-Cryst. Solids **353**, 1713 (2007).
[97] J. N. A. Matthews, Physics Today **61**, 25 (2008).
[98] K. H. Ahn, T. Lookman, A. R. Bishop, Nature **428**, 401 (2004).
[99] S. Tretiak, A. Saxena, R. L. Martin, A. R. Bishop, Proceedings of the National Academy of Sciences of the United States of America **100**, 2185 (2003).
[100] N. K. Voulgarakis, A. Redondo, A. R. Bishop, K. O. Rasmussen, Phys. Rev. Lett. **96** (2006).
[101] J. Barre, A. R. Bishop, T. Lookman, A. Saxena, Phys. Rev. Lett. **94**, 208701 (2005).
[102] O. W. Holmes, The autocrat of the breakfast-table (Phillips, Sampson and Co., Boston, 1858).